Knockout of zebrafish desmin genes does not cause skeletal muscle degeneration but alters calcium flux.

Gulsum Kayman Kurekci[1], Ecem Kural Mangit[1,2], Cansu Koyunlar[1,3], Seyda Unsal[1], Berk Saglam[4], Bora Ergin[4], Ismail Uyanik[5], Niloufar Düz[1], Beril Talim[6], Nuhan Purali[4], Simon M. Hughes[7], Pervin R. Dincer[1]*.

[1]Department of Medical Biology, Hacettepe University Faculty of Medicine, Ankara, 06100, Turkey.

[2]Laboratory Animals Research and Application Centre, Hacettepe University, Ankara, 06100, Turkey

[3]Current address: Department of Hematology, Erasmus MC, Rotterdam, 3015 CN, The Netherlands

[4]Department of Biophysics, Hacettepe University Faculty of Medicine, Ankara, 06100, Turkey.

[5]Department of Electrical and Electronics Engineering, Hacettepe University Faculty of Engineering, Ankara, 06800, Turkey.

[6]Department of Pediatrics, Pathology Unit, Hacettepe University Faculty of Medicine, Ankara, 06100, Turkey.

[7]Randall Centre for Cell and Molecular Biophysics, New Hunt's House, Guy's Campus, King's College London, London, SE1 1UL, United Kingdom.

*Corresponding author.

Abstract

Desmin is a muscle-specific intermediate filament protein that has fundamental role in muscle structure and force transmission. Whereas human desmin protein is encoded by a single gene, two desmin paralogs (*desma* and *desmb*) exist in zebrafish. *Desma* and *desmb* show differential spatiotemporal expression during zebrafish embryonic and larval development, being similarly expressed in skeletal muscle until hatching, after which expression of *desmb* shifts to gut smooth muscle. We generated knockout (KO) mutant lines carrying loss-of-function mutations for each gene by using CRISPR/Cas9. *Desma*;*desmb* double mutants are viable and fertile, and lack obvious skeletal muscle, heart or intestinal defects. In contrast to morphants, knockout of each gene did

not cause any overt muscular phenotype, but did alter calcium flux in myofibres. These results point to a possible compensation mechanism in these mutant lines generated by targeting nonsense mutations to the first coding exon.

Introduction

Desmin is a type III intermediate filament protein that is specifically expressed in skeletal, cardiac and smooth muscles. In addition to their fundamental role in maintaining the structural integrity of the sarcomere, desmin intermediate filaments are involved in mechanotransduction and organelle positioning. Desminopathies belonging to myofibrillar myopathies are primarily characterized by abnormal protein aggregates in muscle and present as progressive skeletal myopathy and/or cardiomyopathy[1]. Although the involvement of smooth muscles is not widely reported, some patients suffer from smooth muscle dysfunction such as swallowing difficulties, intestinal pseudo-obstruction and respiratory insufficiency[2–4]. The majority of desmin mutations are associated with desmin aggregates; however, some mutations have been reported to not alter filament assembly and network integrity *in vivo* or *in vitro*[5,6]. KO of desmin in mice does not affect the viability and the development of muscles; however, muscle degeneration and cardiomyopathy are observed[7,8].

Zebrafish is a widely used model for neuromuscular disorders[9,10]. Besides the advantage of being the most abundant tissue in zebrafish; the gene profile, and the structural and histological features of mammalian skeletal muscle are highly preserved in zebrafish[11]. To date, two approaches have been used to study the effect of the loss of desmin in zebrafish. On one hand, it was shown that morpholino-mediated knockdown of desmin causes skeletal and cardiac muscle myopathy[12,13]. On the other hand, Ramspacher et al. studied a desmin mutant line (*desma*^{sa5}), generated by ENU mutagenesis, which causes a truncation mutation approximately half way along the molecule, that also presented with skeletal and cardiac muscle phenotype[14].

Gene duplications are common in zebrafish and most duplicated genes have similar functions to their human orthologs. Alternatively, paralogs can be expressed in different tissues or stages of development and have distinct functions to their human orthologs. Humans carry a single copy of the *DES* gene whereas two desmin genes (*desma* and *desmb*) are found in zebrafish[13]. Previous work has not established the tissue specific distribution and role of these two desmin paralogs.

Here, we report the spatiotemporal expression pattern of the two desmin paralogs in zebrafish, as well as the generation using CRISPR/Cas9 and characterization of putative null zebrafish mutant lines for each of the desmin paralogs. We show that *desma* and *desmb* are expressed in skeletal muscle until 72-hour post-fertilization (hpf). After 72 hpf, expression of *desmb* shifts to gut smooth muscle. Putative null mutation of each gene does not affect viability and adults do not develop any overt phenotype. However, altered calcium flux was observed in *desma*-KO myofibres. Surprisingly, *desma;desmb* double mutants also survive to adulthood with no sign of muscle defect. These results show that loss-of-function of desmin genes by mutations in the first coding exon result in a mild phenotype with no visible muscle degeneration but altered calcium flux, in contrast to morpholino-mediated knockdown models and the $desma^{sa5}$ allele.

RESULTS

Zebrafish desmin genes

Zebrafish have two *desmin* orthologs, *desma* (*desmin a*) and *desmb (desmin b)*, which are located on chromosome 9 and 6, respectively. *Desma* and *desmb* paralogs share 81% and 83% identity with human *DES* gene. Although a single transcript is known to be encoded by human *DES* gene, in ENSEMBL two isoforms are predicted to be transcribed from *desma*, *desma-1* mRNA coding for a 488 amino acid protein (predicted molecular weight of 55.7 kDa) and *desma-2* mRNA coding for a 473 amino acid protein (predicted molecular weight of 54.1 kDa). In *desma-2* transcript, exon 9 is skipped, corresponding to 15 amino acid located in the tail domain of Desma-1 protein (Supplementary Fig. S1). The 473 amino acid Desmb protein is predicted to have a molecular weight of 54.2 kDa. At the amino acid level, Desma-1, Desma-2 and Desmb show 80%, 82% and 83% similarity with human desmin protein.

Differential expression of desmin transcripts during zebrafish development

We analyzed the spatiotemporal expression patterns of *desma* and *desmb* genes during zebrafish development at several stages beginning from somitogenesis until 5 days post fertilization (dpf) by whole mount *in situ* hybridization (ISH). For detecting both *desma* transcripts (*desma-2* lacks exon 9), we synthesized an antisense probe by using a forward primer binding to exon 1 and a reverse primer binding to exon 10 (Supplementary Fig. S1). No specific staining was observed in embryos treated with sense probes for each gene (Supplementary Fig. S2). *Desma* was first

detected at 11 hpf in adaxial slow muscle precursor cells when the first somites form and remained strongly expressed in somites at all examined stages (Fig. 1a). *Desma* was also expressed in the developing heart from 35 hpf (Fig. 1b). Cryosections of 72 hpf embryos showed that *desma* was distributed in the entire somite, including epaxial and hypaxial muscles (Fig. 1c). By 72 hpf, *desma* was expressed in cranial muscles including external ocular muscles, opercular muscles and mandibular muscles (Fig. 1d). At 96 hpf, transversal sections revealed *desma* expression at the anterior intestine (Fig. 1d, upper panel). At 72, 96 and 120 hpf, expression of *desma* in pectoral fin muscles was clearly visible (Fig. 1d). *Desmb* had an overlapping expression pattern to *desma* from the beginning of somitogenesis until 72 hpf, including staining in trunk somites and heart (Fig. 1a, b). At 72 hpf, somitic expression of *desmb* dramatically decreased with a residual expression in the lateral edges of the myotome. By contrast, strong signal of *desmb* transcripts was detected around the gut throughout the length of the intestine (Fig. 1a, c, e). Similar to *desma*, *desmb* was also expressed in pectoral fin muscles, operculum muscles and mandibular muscles at 72 hpf (Fig. 1e). These results indicate that *desma* and *desmb* expression partially overlap during zebrafish muscle development. As the gut develops, *desmb* expression shifts from somitic muscle to gut smooth muscle.

Generation of *desma* and *desmb* knockout zebrafish lines

Desma and *desmb* mutant zebrafish lines were generated by using CRISPR/Cas9 genome editing. The *desma*^{kg97} line exhibited 2 bp deletion and 4 bp insertion in the first exon (g.198_99delGAinsTGAT, NC_007120.7) leading to a frameshift at amino acid 45 and a premature stop codon after four amino acids. In the *desmb*^{kg156} mutant line, a 5 bp deletion in exon 1 (c.245_249delCTTAT, NM_001077452.1) resulted in a frameshift at amino acid 82 and introduced a premature stop codon after three amino acids (Fig. 2a). Heterozygous mutants showed no defect and homozygous mutant embryos and larvae developed relatively normally, at least for the first few days (Fig. 2b-f).

Expression of *desma* and *desmb* in knockout lines

Mutations were predicted to trigger nonsense-mediated decay of mRNA or synthesis of short truncated polypeptides. As expected, qRT-PCR revealed a significant decrease of *desma* transcripts in *desma*^{kg97} homozygous embryos (P=0.0119, Mann-Whitney U), while *desmb*

transcripts were significantly decreased in *desmb*^{kg156} homozygous embryos at 96 hpf compared to wild type (WT) (P=0.0079, Mann-Whitney U) (Fig. 2b). Consistent with El-Brolosy et al.[15], weak *desmb* or *desma* mRNA up-regulation may occur in the respective mutant embryos (Fig. 2b).

In order to investigate the potential compensatory effect of *desmin* paralog upregulation in mutant embryos, expression patterns of *desmb* and *desma* transcripts were determined in *desma*^{kg97} or *desmb*^{kg156} homozygous mutant embryos, respectively. In *desma*$^{kg97/kg97}$ embryos, the expression pattern of *desmb* transcripts (Fig. 2c) was similar to that of wild-type embryos (Fig. 1a). Somitic expression of *desmb* was observed in *desma*$^{kg97/kg97}$ at 48 hpf, and a shift towards gut expression after 72 hpf. Beyond 72 hpf, no *desmb* staining was detected in somites of *desma*$^{kg97/kg97}$ embryos. In *desmb*$^{kg156/kg156}$ embryos, *desma* was still strongly expressed in somites and visible in the anterior intestine at 96 hpf (Fig. 2c). In order to confirm the loss-of-function of desmin in mutants at the protein level, expression of Desma and Desmb in WT, *desma*^{kg97} or *desmb*^{kg156} homozygous embryos at 96 hpf was determined by immunofluorescent staining using a desmin antibody recognizing both proteins (Fig. 2d-f). In WT embryos, desmin staining was detected in both somites and gut (Fig. 2d). As expected from ISH results, somitic expression was lost and gut was preferentially stained in *desma*$^{kg97/kg97}$ mutants (Fig. 2f). In *desmb*$^{kg156/kg156}$ mutants, expression in somites and anterior intestine were preserved while staining of the middle and posterior intestine was lost (Fig. 2e). We conclude that mutation of each gene reduces the cognate mRNA and protein at all stages examined and that compensation by up-regulation of the unmutated paralogous gene is at best very weak.

General larval characteristics of desmin mutants

In order to evaluate the effects of the absence of *desma* or *desmb* on development, WT, *desma*^{kg97} and *desmb*^{kg156} homozygous embryos/larvae were compared. No significant difference was observed in the number of viable eggs between *desma*$^{kg97/kg97}$ and WT (P=0.6842, Mann-Whitney U) or *desmb*$^{kg156/kg156}$ and WT (P=0.9654, Mann-Whitney U) (Fig. 3a). Hatching period (48-72 hpf[16]) is a critical process in embryonic development and reduction in the hatching rate could be associated with reduced muscle function[17]. The time course showed that although different hatching times were observed between groups, no significant difference was found between hatching rates of mutant and WT embryos at 72 hpf with over 94% of embryos hatched

(*desma*$^{kg97/kg97}$ vs. WT, *P*=0.9902; *desmb*$^{kg156/kg156}$ vs WT, *P*=0.3186, repeated measures two-way ANOVA, Bonferroni post *hoc* test) (Fig. 3b).

Similar mortality rates were observed with no significant difference between homozygous mutants of *desma*^{kg97} or *desmb*^{kg156} and WT embryos (*desma*$^{kg97/kg97}$ vs. WT, *P*=0.1287; *desmb*$^{kg156/kg156}$ vs. WT, *P*=0.6239, repeated measures two-way ANOVA) (Fig. 3d). Finally, among surviving larvae, no statistically significant difference in body length was observed between WT and mutant groups (*P*=0.2036 for WT vs. *desma*$^{kg97/kg97}$; *P*=0.1893 for WT vs. *desmb*$^{kg156/kg156}$, Mann-Whitney U) (Fig. 3c).

Mutant larvae show no neuromuscular defect

Muscle fibre integrity and somite morphology length were investigated by staining muscle actin with rhodamine phalloidin in 96 hpf embryos (Fig. 3e). At this stage, mainly *desma* is expressed in somites. No muscle lesion or detachment of fibres was observed in mutants and no significant difference was found in somitic length between mutants and WT (*P*=0.7912 for WT vs. *desma*$^{kg97/kg97}$; *P*=0.4923 for WT vs. *desmb*$^{kg156/kg156}$, Mann-Whitney U) (Fig. 3f).

Touch-evoked response assay is a widely used method to assess neuromuscular function in 48 hpf zebrafish embryos[18]. We performed motility experiments in a blinded manner on siblings from three groups of heterozygous mutant in-crosses and genotyped them after. First, the average escape time of siblings from *desma*$^{kg97/+}$ in-crosses was assessed and no significant difference was found in *desma*^{kg97} heterozygous (*P*=0.122, Mann-Whitney U) or homozygous (*P*=0.5529, Mann-Whitney U) mutants compared to WT (Fig. 3g). Similarly, no significant difference in the average escape time was found in *desmb*^{kg156} heterozygous (*P*=0.3968, Mann-Whitney U) or homozygous (*P*=0.6131, Mann-Whitney U) mutants compared to WT (Fig. 3h). Since both *desma* and *desmb* are expressed in somites up to this stage (48 hpf) and might potentially compensate for the absence of each other, we finally evaluated the effect of the absence of both proteins in siblings from *desma*$^{kg97/+}$;*desmb*$^{kg156/kg156}$ double mutants. No significant difference in the average escape time was found in homozygous double mutants (*desma*$^{kg97/kg97}$;*desmb*$^{kg156/kg156}$) compared to *desma*$^{+/+}$;*desmb*$^{kg156/kg156}$ (*P*=0.3165, Mann-Whitney U) and in *desma*$^{kg97/+}$;*desmb*$^{kg156/kg156}$ embryos compared to *desma*$^{+/+}$;*desmb*$^{kg156/kg156}$ (*P* = 0.2334, Mann-Whitney U) (Fig. 3i).

Mutant adult skeletal muscle shows no muscle degeneration

Because no skeletal muscle phenotype was observed in mutant larvae, surviving one-year-old adults were investigated for muscle defects. Some homozygous single and double mutants survived until adulthood with no sign of behavioral defect. Western blot was performed using myotomal skeletal muscle protein extracts isolated from adult fish (WT, homozgous and heterozygous *desma*^{kg97} mutants, homozygous and heterozygous *desmb*^{kg156} mutants and *desma*$^{kg97/kg97}$;*desmb*$^{kg156/kg156}$ double mutants). As *desma* was shown to be predominantly expressed in somites from 72 to 120 hpf, the two bands detected in WT and *desmb*^{kg156} mutants were predicted to correspond to Desma-1 (predicted molecular weight 55.7 kDa) and Desma-2 (predicted molecular weight 54.1 kDa) isoforms. In agreement with that, both bands were absent in *desma*^{kg97} homozygous mutant and double mutants while still expressed in homozygous *desmb*^{kg156} mutant (Fig. 4a). Nevertheless, histopathological examination of hematoxylin-eosin stained skeletal muscle tissue sections revealed no pathological changes in homozygous single or double mutants (Fig. 4b). General morphology of skeletal fibre shape and size, integrity of sarcoplasm was normal. There was an absence of cytoplasmic aggregates, signs of degeneration or regeneration, internal nuclei, inflammatory cell infiltration, increase in connective or adipose tissue in interstitium (Fig. 4b). We conclude that fish entirely lacking wild-type desmin generate and maintain functional skeletal muscle in the context of a zebrafish aquarium.

Altered calcium flux in *desma* mutant fibres

Although anatomically apparently wild-type, adult *desma*$^{kg97/kg97}$ mutants were physiologically defective in calcium handling. To investigate amplitude and time course of calcium signals released in response to a depolarizing voltage stimulus, individual fibres were dissected from WT (N=8), *desma*^{kg97} (N=11) or *desmb*^{kg156} (N=8) homozygous mutant 1-year-old fish. Calcium flux along fibres was monitored in the isolated fibres by Fluo-4 AM after four consecutive depolarizing stimuli with the amplitude of the current pulse kept constant at 100 nA and the duration increased by 10 ms at each pulse (Fig. 5a-b). Amplitudes of the calcium emission signals in the first (10 ms) stimulus and fourth (40 ms) stimulus were compared between mutants and WT. To eliminate variance induced by amplitude, offset and fibre size differences, amplitude values were baseline corrected and divided by the diameter of each fibre. Amplitudes of the first or the fourth calcium transient were significantly lower in *desma*$^{kg97/kg97}$ fibres compared to WT fibres (P=0.0008 for

first transient; P=0.0025 for fourth transient, Mann-Whitney U) (Fig. 5c-d). In contrast, no significant difference was found in the amplitude of calcium flux between *desmb*$^{kg156/kg156}$ fibres and WT fibres (P=0.0881 for first transient; P=0.6657 for fourth transient, Mann-Whitney U) (Fig. 5c-d).

Time course of the longest calcium transient (40 ms, fourth transient) has been analyzed for comparing the waveform of the responses and dissecting each phase of the transient. Signals have been baseline corrected and then normalized. Mean amplitude values as a function of time were compared between *desma*$^{kg97/kg97}$ and WT or *desmb*$^{kg156/kg156}$ and WT. No significant difference was found in the rising and the plateau phases of the recorded transients between the experimental groups (Figure 5e). However, the decay phase was significantly faster in *desma*$^{kg97/kg97}$ mutant fibres compared to WT (* indicates P<0.05, repeated measures ANOVA, Bonferroni post *hoc* test). No significant difference was found in *desmb*$^{kg156/kg156}$ mutant fibres compared to WT (Fig. 5e).

DISCUSSION

We demonstrated differential expression of *desma* and *desmb* paralogs during zebrafish development. Although previous studies showed that *desma* is the main gene expressed in somites, no study did clearly distinguish the spatial and temporal differences in the expression of the two genes. We showed that until 72 hpf *desma* and *desmb* expression overlap but later in development, their expression diverges. While *desmb* expression shifts from somites to gut, *desma* remains as the predominantly expressed paralog in somites. Note that the residual *desmb* expression detected in the lateral edges of the myotome might reflect a transient expression in new muscle fibres[19]. Reduction of Desmin protein in adult *desma* mutants confirms that Desma is the major desmin protein in adult zebrafish skeletal muscle. Desmb appears the major desmin in smooth muscle, at least in the gut. So zebrafish *desmb* mutants may be particularly useful for understanding the role of desmin in smooth muscle without interference by additional phenotypes from skeletal muscle. In future studies, it will be necessary to take into account this divergent expression when studying the role of desmin in zebrafish.

Reduced *desma* or *desmb* mRNAs in their respective mutants suggest the mRNAs are degraded by nonsense-mediated decay, such that only tiny amounts of the severely truncated proteins would be produced. Such fragments lack the highly conserved α-helical central rod

domain responsible for filament formation and all known protein-protein interaction domains of Desmin[20]. Intriguingly, no overt phenotype was observed in some double homozygous mutants. In contrast to desmin morphants where both *desma* and *desmb* were targeted with morpholinos [13], we found that *desma*^{kg97} or *desmb*^{kg156} alleles have no effect on hatching of eggs, mortality rate and length of larvae. While motility is altered in 48 hpf desmin morphants, no significant alteration was detected in *desma*^{sa5} embryos[13,21]. By reasoning that this could be due to a compensation by *desmb*, which is still expressed in somites at 48 hpf, we performed motility assays in both single mutant and double mutant embryos but found no additional neuromuscular defect in larvae mutant in single or both desmin genes. At the histological level, no sign of muscle degeneration or disorganisation of fibres was observed in *desma*^{kg97} or *desm*b^{kg156} mutant skeletal muscles in either embryos and adults. In contrast, the desmin morphants and *desma*^{sa5} mutant muscles of embryos were disorganized, with disruption of sarcomeres[13,14]. Our findings raise the possibility that a haploinsufficient dominant effect in *desma*^{sa5} mutants may disrupt muscle; such an explanation would no account for the morphant phenotype. We conclude that at least two further alleles of *desma* may be needed to resolve these differences: firstly, a deletion allele that would simultaneously prevent any Desma polypeptide synthesis and any RNA-triggered compensation and, secondly, an allele lacking morpholino binding ability but nevertheless encoding wild-type protein to prove that the morphant phenotype is due to *desma* binding.

We found that the amplitude of calcium signals released in response to a depolarizing current stimulus applied to fibres was significantly lower in *desma*^{kg97} compared to WT. In addition, while rising and plateau phases of calcium signals were similar between all groups, the decay phase was shorter in *desma*^{kg97} mutants compared to WT. These results indicate that mechanisms regulating cytosolic calcium are altered and fibres are not efficient in generating a long lasting calcium increase in the absence of desmin. These results are concordant with calcium flux defects observed in desmin mutant mice and hearts of *desma*^{sa5} embryos[14]. Our data support the idea that desmin has a similar role in calcium conduction in skeletal muscle fibres and suggest that some aspects of the *desma*^{sa5} phenotype may reflect loss of function of Desma.

Although not the focus of this study, it should be noted that heart and gastroinstestinal development in mutant lines have not been extensively analyzed. No heart oedema such as observed in desmin morphant or overt morphological abnormality in the gut have been observed in *desma*^{kg97}, *desmb*^{kg156} or double mutant embryos and adults.

Many loss-of-function mutants not exhibiting an overt phenotype and failing to phenocopy morphants have been previously reported[22–24]. El-Brolosy et al. proposed transcriptional adaptation triggered by mutant RNA degradation as a mechanism to explain this discrepancy[15,25]. According to this model, decay of the mutant mRNA results in upregulation of related genes, alleviating or suppressing the phenotype observed in morphants. Such adaptation could explain the milder phenotype observed in mutants created in our study compared to desmin morphants. However, it has been shown that *desma*^{sa5} allele results in a muscle phenotype similar to that of morphants, even though the *desma*^{sa5} allele predicts an in-frame stop codon and no *desma* mRNA was detected in mutants[14,21]. We also observe a severe reduction in *desma* mRNA in our *desma*^{kg97} mutant. The specific mechanism leading to the absence of mRNA was not investigated either in *desma*^{sa5} mutants or in the present study. It is possible that the *desma*^{sa5} allele is not as efficient as *desma*^{kg97} allele in triggering an adaptation mechanism for yet unknown reasons. However, our data suggest that the compensating gene in fish carrying our *desma* allele is not *desmb*, the only gene known to have high and extensive homology to *desma*. It will be interesting to compare these models in the contexts of mRNA decay and transcriptional adaptation. Alternatively, short truncated polypeptides not detected in Western blot might play a role in this process before being rapidly degraded. In conclusion, unraveling modifier genes and proteins that compensate for the loss of desmin in our models will bring further insights in the role of desmin in muscle.

METHODS

Ethical approval and zebrafish maintenance

All animal procedures were approved by the Hacettepe University Animal Experimentations Local Ethics Board (2014/07-08). Adult zebrafish (AB) (*Danio rerio*) were kept in 14/10 hr light-dark cycle at 28.5^{o}C. Adults are fed twice a day, with dry feed in morning and *Artemia spp.* in evening. For spawning, male and female fish were placed in a breeding tank with a separator. Next morning the separator was removed, viable eggs were collected and rinsed in E3 medium (5 mM NaCl, 0.17 mM KCl, 0.33 mM $CaCl_2$, 0.33 mM $MgSO_4$, 10^{-5}% Methylene Blue). Embryos were kept in E3 medium for five days and placed into adult tanks containing system water. Embryos were fed five times a day with dry feed and Artemia.

Whole mount *in situ* hybridization

Embryos were fixed in 4% PFA in PBS (w/v) overnight at 4°C, dehydrated in 50% and %100 methanol washes and stored at -20°C at least overnight before use. Probe templates were amplified from cDNA isolated from 96 hpf wild-type embryos. Reverse primers for antisense probe contained T3 promoter sequence while forward primers for sense probes contained T7 promoter sequence. Primers sequences can be found as Supplementary Table S1 online. Digoxigenin-labelled probes were generated using T3 or T7 RNA polymerases. Whole mount *in situ* mRNA hybridization was performed as described[26]. Embryos were photographed as on Zeiss Axiophot with Axiocam (Carl Zeiss, Oberkochen, Germany) using Openlab software (Agilent, Santa Clara, CA, USA).

Generation of mutant zebrafish lines

CRISPR-Cas9 genome editing was performed as described in Fin et al[24]. CRISPR-Cas9 sgRNAs showing minimal off-target sites were designed by using the online software ZiFiT Targeter. Oligos encoding sgRNAs targeting the first exon of *desma* (GRCz11, Chr9: 7539113-7539132, GGTCACCTCGTAAACTCTGG) and *desmb* (GRCz11, Chr6: 13891417-13891437, GGCTATACTCGCTCTTATGG) were cloned into pDR274 plasmid (Addgene). sgRNAs were synthesized using T7 RiboMAX Large Scale RNA production system (Promega) following the manufacturer's protocol. Transcribed sgRNAs were purified using sodium acetate and ethanol precipitation and quantified on Qubit fluorometer. Cas9 mRNA was transcribed from pCS2-Cas9 plasmid using mMessage mMachine SP6 Kit (Ambion) and purified by lithium chloride precipitation. One-cell stage embryos were injected with 2 nl containing 80-200 pg of sgRNA and 100 pg of Cas9 mRNA. At 48 hpf, ten embryos were analysed for mosaicism at targeted loci using high resolution melt analysis. Injected embryos were raised to adulthood and back-crossed to identify transmitted mutations in F1 progeny. Homozygotes for each gene were generated by in-cross of F2 heterozygotes. Primers sequences used for genotyping by Sanger sequencing can be found as Supplementary Table S1 online.

Quantitative real-time PCR

Total RNA was isolated from a pool of 20 mechanically homogenized embryos at 96 hpf for each sample (n=8) using TRItidy G (AppliChem) and 500 ng of cDNA was synthesized using QuantiTect Reverse Transcription Kit (Qiagen) according to manufacturer's protocol. Primer

sequences for *desma* (covering both *desma-1* and *desma-2*), *desmb* and *actb1* can be found as Supplementary Table S1 online. qPCR was performed in triplicates using SensiFAST SYBR No-ROX Kit (Bioline) in Rotor-Gene 6000 (Corbett Life Science). *Desma* and *desmb* expression levels were normalized to *actb1* expression, mutant expression levels were calculated relative to wild-type using ΔΔCt method[27].

Protein Extraction and Immunoblotting

For protein extraction, 1-year-old fish were euthanized using overdose of tricaine (MS222, 300 mg/l). Skeletal muscle tissue was immediately dissected and fresh-frozen in liquid nitrogen. Tissue was pulverized and homogenized in blending buffer (16 M Tris HCl, 200 M EDTA, 20% SDS, 1X protease inhibitor cocktail, volume adjusted to 5 ml with dH_2O) by sonication on ice. Lysates were then centrifuged and supernatant transferred in a fresh tube. Total protein concentrations were determined by bicinchoninic acid Protein Assay (Pierce, 23225). Equal amounts of protein (40 µg) were loaded on a 13% polyacrylamide gel and transferred onto a nitrocellulose membrane using semi-dry transfer, blocked for one hour at room temperature (%5 nonfat dried milk in %0,2 TBS-T) and probed with anti-desmin antibody (1:1000; Sigma, D8281) overnight at 4°C or anti-lamin B1 antibody (Abcam, ab90169) followed by appropriate HRP-conjugated secondary antibody. Chemiluminescence detection was done by using SuperSignal™ West Femto Maximum Sensivity substrate (Thermo Scientific, 34095) in GeneGnome device.

Whole-mount Immunofluorescence

96 hpf embryos were fixed in %4 PFA overnight at +4°C and washed with PBTx (%0.01 Triton X-100 in PBS). Embryos were permeabilized in 50 µg/ml Proteinase K for 2 hours and re-fixed in 2% PFA for 20 minutes at room temperature. Embryos were blocked in %5 BSA for 2 h at room temperature and incubated with anti-desmin antibody (1:20; Sigma, D8281) for two overnights. After two overnight incubations with Alexa-Fluor 488 conjugated secondary antibody, embryos were mounted with DAPI onto glass bottom dishes for imaging with Zeiss LSM Pascal laser scanning confocal microscope.

Larval Phenotype and Morphology

After successful mating, embryos were collected, counted and recorded for the following rates. Hatching rate was reported as cumulative percentage of hatched embryos at 24 hpf, 48 hpf and 72

hpf. Mortality rate was expressed as the percentage of death embryos for 5 dpf. For body length measurements, at least 16 embryos at 96 hpf were mounted, photographed (The Imaging Source, DFK 41AU02) and measured from the mouth tip to the tail base using ImageJ (Version 1.49u). Values for body length were presented as mean body length in cm. All the experiments except body length measurements (three times) were performed at least eight times.

Phalloidin Staining

Phalloidin staining was performed on 96 hpf embryos (N=8) as described[28]. Following fixation in 4% PFA and permeabilization with 50 µg/ml Proteinase K, embryos were incubated in Alexa-Fluor 488 conjugated Phalloidin (Invitrogen, A12379) overnight at +4ºC. Embryos were then mounted onto glass bottom dishes and photographed with Zeiss LSM Pascal laser scanning confocal microscope. Somite lengths were measured by using ImageJ (Version 1.49u).

Hematoxylin Eosin Staining

Adult zebrafish were freshly frozen in methyl-butanol cooled down in liquid nitrogen and then taken into O.C.T compound for sectioning. Tissue sections were incubated in hematoxylin for 5 minutes, 1% acid-alcohol solution for 1 minute, 1% ammoniac for 1 minute, eosin solution for 3 minutes respectively by washing with distilled water in between steps. Finally, sections were washed with alcohol and xylene, and mounted. Sections were scanned with Nikon Eclipse E-400 microscope and photographed by DXM 1200F digital camera.

Motility Assay

For motility assay 48 hpf embryos from in-crosses of *desma*$^{kg97/+}$, *desmb*$^{kg156/+}$ or *desma*$^{kg97/+}$;*desmb*$^{kg156/kg156}$ adults were used. Motility assays were performed by previously described protocol[18]. A petri dish was placed on a transparent sheet with concentric circles 5 mm apart. One embryo at a time was positioned in the centre of the dish and stimulated using a dissection needle. The escape response of the embryo was recorded using a high-speed camera (Huawei, Mate 10 Lite, 16 MP, 120 fps). The movements of the embryo—midpoint between the two eyes—were tracked using a custom software that works based on template matching algorithm. The elapsed time between the last frame before touch stimulus and the first frame after the body of the fish contacts the 10 mm circle was computed from the digitized embryo movements

with a resolution of 8.3 ms (120 fps). Experiments were performed blindly and after video accusation, DNA was extracted from each embryo for genotyping.

Calcium Flux

1-year-old fish were euthanized using overdose of tricaine (MS222, 300 mg/l). After removal of the skin, tissue samples were incubated into 5 mg/ml collagenase solution in PBS (without Ca^{2+} and Mg^{2+}) at 28.5 °C for 20 minutes on a shaker at 50 rpm. Samples have been triturated gently under dissecting microscope in order to dissociate muscle fibres from the tissue components until rode-shaped muscle fibres were obtained. Dissociated fibres were incubated in DMEM containing 10% FBS and 1% antibiotic-antimycotic overnight at 28.5 °C and 5% CO_2 environment. On the following day, fibres were incubated in 2.5 µM Fluo-4 AM for 20 minutes in 5% CO_2. Under a laser scanning confocal microscope (Zeiss LSM Pascal), glass microelectrodes (filled with 3M KCl) were inserted into muscle fibres in a current clamp mode[29]. A depolarizing current stimulus was delivered through the microelectrode to excite the fibre and evoke a calcium signal. The evoked calcium-specific fluorescent emission signal was recorded in "Line Scan" mode of confocal microscope, supplying information about a line cross sectioning the muscle fibre at a high frequency in tandem with the electrical recordings. Data were analyzed in MATLAB (The MathWorks, Inc). The stimulus waveform, which consisted of four consecutive pulses increasing in duration, was used in all the experiments. The amplitude of the current pulse was kept constant at 100 nA while the durations were 10 ms, 20 ms, 30 ms, 40 ms respectively. Experiments were done by using three WT, three *desma*$^{kg97/kg97}$ and two *desmb*$^{kg156/kg156}$ fish and at least eight fibres from each group were recorded.

Statistics

Data were statistically analyzed by GraphPad Prism 8 (GraphPad Software Inc.) by nonparametric Mann-Whitney U test (Two-tailed) when two groups were compared. The results were considered significant when $P<0.05$. For analysis of time course experiments (hatching rate, mortality rate and time course calcium flux), repeated measures two-way ANOVA was used and Bonferroni post *hoc* test was used for multiple comparisons. All error bars were presented as mean±SEM and bars were represented as median.

Acknowledgements

This work was supported by The Scientific and Technological Research Council of Turkey, Project no. 214S174 to P.R.D.

Competing interests

The author(s) declare no competing interests.

Author Contributions

P.R.D. designed, P.R.D. and S.M.H. supervised the study. G.K.K. wrote the paper, E.K.M. made contribution to writing the paper and assembled the figures. G.K.K., E.K.M, C.K., S.U., B.S., B.E., I.U., N.D., B.T. and N.P. performed the experiments and/or analyzed the results. All authors interpreted the data and edited the manuscript.

Data Availability

Supporting information is available in Supplementary files and further information is available from the corresponding author upon request.

References

1. Clemen, C. S., Herrmann, H., Strelkov, S. V. & Schröder, R. Desminopathies: Pathology and mechanisms. *Acta Neuropathologica* (2013) doi:10.1007/s00401-012-1057-6.
2. Dagvadorj, A. *et al.* Respiratory insufficiency in desminopathy patients caused by introduction of proline residues in desmin C-terminal α-helical segment. *Muscle and Nerve* (2003) doi:10.1002/mus.10370.
3. Ariza, A. *et al.* Desmin myopathy: a multisystem disorder involving skeletal, cardiac, and smooth muscle. *Hum. Pathol.* (1995) doi:10.1016/0046-8177(95)90095-0.
4. Goldfarb, L. G. *et al.* Missense mutations in desmin associated with familial cardiac and skeletal myopathy. *Nat. Genet.* (1998) doi:10.1038/1300.
5. Cetin, N. *et al.* A novel desmin mutation leading to autosomal recessive limb-girdle muscular dystrophy: distinct histopathological outcomes compared with desminopathies. *J. Med. Genet.* **50**, 437–43 (2013).
6. Bär, H. *et al.* Conspicuous involvement of desmin tail mutations in diverse cardiac and

skeletal myopathies. *Hum. Mutat.* (2007) doi:10.1002/humu.20459.

7. Li, Z. *et al.* Cardiovascular lesions and skeletal myopathy in mice lacking desmin. *Dev. Biol.* (1996) doi:10.1006/dbio.1996.0122.

8. Milner, D. J., Weitzer, G., Tran, D., Bradley, A. & Capetanaki, Y. Disruption of muscle architecture and myocardial degeneration in mice lacking desmin. *J. Cell Biol.* (1996) doi:10.1083/jcb.134.5.1255.

9. Lin, Y. Y. Muscle diseases in the zebrafish. *Neuromuscular Disorders* (2012) doi:10.1016/j.nmd.2012.04.007.

10. Berger, J. & Currie, P. D. Zebrafish models flex their muscles to shed light on muscular dystrophies. *Dis. Model. Mech.* **5**, 726–32 (2012).

11. Gibbs, E. M., Horstick, E. J. & Dowling, J. J. Swimming into prominence: the zebrafish as a valuable tool for studying human myopathies and muscular dystrophies. *FEBS J.* **280**, 4187–97 (2013).

12. Vogel, B. *et al.* In-vivo characterization of human dilated cardiomyopathy genes in zebrafish. *Biochem. Biophys. Res. Commun.* **390**, 516–522 (2009).

13. Li, M., Andersson-Lendahl, M., Sejersen, T. & Arner, A. Knockdown of desmin in zebrafish larvae affects interfilament spacing and mechanical properties of skeletal muscle. *J. Gen. Physiol.* **141**, 335–345 (2013).

14. Ramspacher, C. *et al.* Developmental Alterations in Heart Biomechanics and Skeletal Muscle Function in Desmin Mutants Suggest an Early Pathological Root for Desminopathies. *Cell Rep.* **11**, 1564–76 (2015).

15. El-Brolosy, M. A. *et al.* Genetic compensation triggered by mutant mRNA degradation. *Nature* **568**, 193–197 (2019).

16. Kimmel, C. B., Ballard, W. W., Kimmel, S. R., Ullmann, B. & Schilling, T. F. Stages of Embryonic Development of the Zebrafish. *Dev. Dyn.* **203**, 253–310 (1995).

17. Skobo, T. *et al.* Zebrafish ambra1a and ambra1b knockdown impairs skeletal muscle development. *PLoS One* (2014) doi:10.1371/journal.pone.0099210.

18. Goody, M. F. *et al.* NAD+ Biosynthesis Ameliorates a Zebrafish Model of Muscular Dystrophy. *PLoS Biol.* (2012) doi:10.1371/journal.pbio.1001409.

19. Campbell, J. M., Hartjes, K. a, Nelson, T. J., Xu, X. & Ekker, S. C. New and TALENted genome engineering toolbox. *Circ. Res.* **113**, 571–87 (2013).

20. Hnia, K., Ramspacher, C., Vermot, J. & Laporte, J. Desmin in muscle and associated diseases: beyond the structural function. *Cell and Tissue Research* (2015) doi:10.1007/s00441-014-2016-4.

21. Ramspacher, C. *et al.* Developmental Alterations in Heart Biomechanics and Skeletal Muscle Function in Desmin Mutants Suggest an Early Pathological Root for Desminopathies. *Cell Rep.* **11**, 1564–1576 (2015).

22. Kok, F. O. *et al.* Reverse genetic screening reveals poor correlation between morpholino-induced and mutant phenotypes in zebrafish. *Dev. Cell* (2015) doi:10.1016/j.devcel.2014.11.018.

23. Law, S. H. W. & Sargent, T. D. The serine-threonine protein kinase PAK4 is dispensable in zebrafish: Identification of a morpholino-generated pseudophenotype. *PLoS One* (2014) doi:10.1371/journal.pone.0100268.

24. Fin, L., Bergamin, G., Steiner, R. A. & Hughes, S. M. The Cannabinoid Receptor Interacting Proteins 1 of zebrafish are not required for morphological development, viability or fertility. *Sci. Rep.* **7**, 1–9 (2017).

25. Rossi, A. *et al.* Genetic compensation induced by deleterious mutations but not gene knockdowns. *Nature* **524**, 230–233 (2015).

26. Hinits, Y. & Hughes, S. M. Mef2s are required for thick filament formation in nascent muscle fibres. *Development* (2007) doi:10.1242/dev.007088.

27. Schmittgen, T. D. & Livak, K. J. Analyzing real-time PCR data by the comparative CT method. *Nat. Protoc.* (2008) doi:10.1038/nprot.2008.73.

28. Goody, M. & Henry, C. http://www.bio-protocol.org/e786 Vol 3, Iss 11, Jun 05, 2013. *Bio-Protocol* (2013).

29. Purali, N. Fast calcium transients translate the distribution and conduction of neural activity in different regions of a single sensory neuron. *Invertebr. Neurosci.* (2017) doi:10.1007/s10158-017-0201-3.

Figure Legends

Fig. 1. Whole mount *in situ* mRNA hybridisation of embryos at the indicated stages for antisense probes to *desma* and *desmb*. (**a**) Lateral views are anterior to top, dorsal to left for 13-22 hpf; anterior to left except 11 hpf which is a dorsal view. 48-120 hpf whole mounts are anterior to left, dorsal to top. Scale bar: 250 µm. (**b**) Arrows indicate heart in frontal view for left panel (*desma*) and ventral view for right panel (*desmb*) of 35 hpf embryos. (**c**) Transversal sections where dorsal is top. (**d**) Upper left panel is a lateral view at 96 hpf, scale bar: 250 µm. Dashed line represents the position of the transversal section in upper right panel where dorsal is top, scale bar: 100 µm. Lower panels are lateral views of zebrafish heads at 72 and 120 hpf treated with *desma* probe. Scale bar: 100 µm. (**e**) Left panel is a ventral view with anterior at top. Right panels are lateral views. Ai, anterior intestine; eom, extraocular muscles; fast, fast muscles; fm, pectoral fin muscles; hm, hypaxial muscles; mdm, mandibular muscles; om, opercular muscles; slow, slow muscles; som, somites. Scale bar: 250 µm.

Fig. 2. Generation of *desma* and *desmb* knockout lines. (a) Alignments and chromatograms of wild-type DNA sequences with mutant alleles, and predicted mutant polypeptide sequences. In DNA sequences, yellow highlights gRNA target sequence, hyphens show deleted bases, inserted bases are indicated in red font. In protein sequences, the first residue affected by the frameshift is indicated in red font, asterisks represent early stop codons. (**b**) Quantitative real-time PCR results showing the expression of *desma* mRNA (upper graphic) and *desmb* mRNA (lower graphic) in wild-type and homozygous mutant 96 hpf embryos (N=5). A significant decrease of *desma* transcripts in $desma^{kg97}$ homozygous embryos (P=0.0119, Mann-Whitney U) was observed while *desmb* transcripts were significantly decreased in $desmb^{kg156}$ homozygous embryos at 96 hpf compared to WT (P=0.0079, Mann-Whitney U). (**c**) Left panel shows whole mount *in situ* mRNA hybridisation of $desma^{kg97}$ homozygous embryos at the indicated stages for antisense probes to *desmb*. Right panel shows whole mount *in situ* mRNA hybridisation of $desmb^{kg156}$ homozygous embryos at the indicated stages for antisense probes to *desma.* Scale bar: 250 µm. Ai, anterior intestine; som, somites. (**d-f**) Whole mount immunofluorescence staining of desmin with an anti-desmin polyclonal antibody (Sigma, D8281) recognizing both Desma and Desmb, in wild-type and mutant 96 hpf embryos. Scale bar: 500 µm. Boxes with dashed lines delineate areas that were

zoomed and focused on intestine. Pictures showing DAPI staining of each embryo are included at their bottom right. (**d**) Upper panel is lateral view of a WT embryo with anterior to left, dorsal to top. Lower panel is ventral view with anterior to left, arrowheads indicate the gut. (**e**) Upper panels are lateral views of *desmb*$^{kg156/kg156}$ embryo with anterior to left, dorsal to top. Lower left panel shows anterior intestine (orange arrowheads), lower right panel shows middle and posterior intestine (white arrowheads). (**f**) Lateral view of *desma*$^{kg97/kg97}$ with anterior to left, dorsal to top.

Fig. 3. Evaluation of neuromuscular defect in mutant larvae. (**a)** The number of viable embryos after successful mating of WT fish (n=10) compared to homozygous *desma*^{kg97} (n=10) (*P*=0.6842, Mann-Whitney U) or homozygous *desmb*^{kg156} (n=8) (*P*=0.9654, Mann-Whitney U) fish. (**b)** Comparison of hatching rate between homozygous mutants and WT 24, 48 and 72 hpf embryos At 72 hpf, no significant difference in the hatching rate was found between mutants and WT (*desma*$^{kg97/kg97}$ vs. WT, *P*=0.9902; *desmb*$^{kg156/kg156}$ vs WT, *P*=0.3186, repeated measures two-way ANOVA, Bonferroni post *hoc* test) (**c)** Body length of 96 hpf WT (N=18) and homozygous *desma*^{kg97} (N=25) or homozygous *desmb*^{kg156} (N=16) mutant embryos (*P*=0.2036 for WT vs. *desma*$^{kg97/kg97}$; *P*=0.1893 for WT vs. *desmb*$^{kg156/kg156}$, Mann-Whitney U). (**d)** Cumulative mortality rate from 1 to 5 dpf homozygous *desma*^{kg97} mutants (N=1247) compared to WT (N=2460) (*P*=0.1287, repeated measures two-way ANOVA, Bonferroni post *hoc* test) and homozygous *desmb*^{kg156} mutants (N=2615) compared to WT (*P*=0.6239, repeated measures two-way ANOVA, Bonferroni post *hoc* test). **e.** Optical sections of the mid-trunk region of WT and homozygous mutants 96 hpf embryos stained with phalloidin (N=8). Scale bars: 50 µm. (**f)** Somite lengths (µm, N=8) were measured from optical sections of WT and mutant embryos stained with phalloidin (*P*=0.7912 for WT vs. *desma*$^{kg97/kg97}$; *P*=0.4923 for WT vs. *desmb*$^{kg156/kg156}$, Mann-Whitney U). (**g-i)** Touch-evoked escape time (ms) of 48 hpf embryos. Motility experiments were performed blind on siblings from (**g**) *desma*$^{kg97/+}$, (**h**) *desmb*$^{kg156/+}$ or (**i**) *desma*$^{kg97/+}$;*desmb*$^{kg156/kg156}$ in-crosses followed by *post hoc* genotyping. g. Heterozygous *desma*^{kg97} embryos (N=23) were compared to WT (N=9) (P=0.122, Mann-Whitney U) and *desma*$^{kg97/kg97}$ (N=15) compared to WT (P=0.5529, Mann-Whitney U). h. Heterozygous *desmb*^{kg156} embryos (N=6) were compared to WT (N=38) (P=0.3968, Mann-Whitney U) and *desmb*$^{kg156/kg156}$ (N=6) compared to WT (P=0.6131, Mann-Whitney U). i. Homozygous double mutants (N=8) were compared to *desma*$^{+/+}$;*desmb*$^{kg156/kg156}$ (n=15) (*P*=0.3165, Mann-Whitney U) and *desma*$^{kg97/+}$;*desmb*$^{kg156/kg156}$ embryos (n=34) compared to *desma*$^{+/+}$;*desmb*$^{kg156/kg156}$ (*P*=0.2334, Mann-Whitney U).

Figure 4. **Desmin protein expression and histological examination of adult skeletal muscle.** **(a)** Immunoblotting of skeletal muscle protein extracts of WT, *desma*$^{kg97/kg97}$, *desma*$^{kg97/+}$, *desmb*$^{kg156/kg156}$, *desmb*$^{kg156/+}$ and *desma*$^{kg97/kg97}$;*desmb*$^{kg156/kg156}$ double mutant fish, showing expression of putative Desma-1 (55.7 kDa) and Desma-2 (54.1 kDa) isoforms. Lamin B1 was labeled as loading control. (**b)** Transversal cryosections of mid-trunk somites from WT and homozygous single and double mutant adults stained with hematoxylin eosin showing no pathological changes. Scale bar: 250 µm.

Fig. 5. Calcium flux in isolated fibres. (**a**) Calcium flux along fibres was monitored in vivo by Fluo-4 AM after four consecutive depolarizing stimuli. Top panel, membrane potential responses to current stimulus pulses with varying durations of 10, 20, 30, 40 ms with the amplitude of the current pulse kept constant at 100 mV and the duration increased by 10 ms at each pulse. Middle panel, evoked calcium transients in line scan mode (*tx*) to current stimuli. Bottom panel, integrated emission signal as a function of time for each experimental group. (**b**) Membrane potential response to the first stimulus of 10 ms (top) or to the fourth stimulus of 40 ms. (**c**) Baseline corrected amplitude divided by fibre diameter (ΔF/µm) of the calcium emission signals during the first (10 ms) stimulus and fourth (40 ms) stimulus were compared between mutants and WT. (**e**) Time course analysis of the baseline corrected and normalized amplitude of the calcium transient from the longest stimulus (40 ms) was represented as mean amplitude values as a function of time. Homozygous *desma*^{kg97} fibres (N=11, red curve) or homozygous *desmb*^{kg156} fibres (N=8, orange curve) were compared to WT (N=8, blue curve). (* indicates time points where $P<0.05$, repeated measures two-way ANOVA, Bonferroni post *hoc* test).

Figure 1.

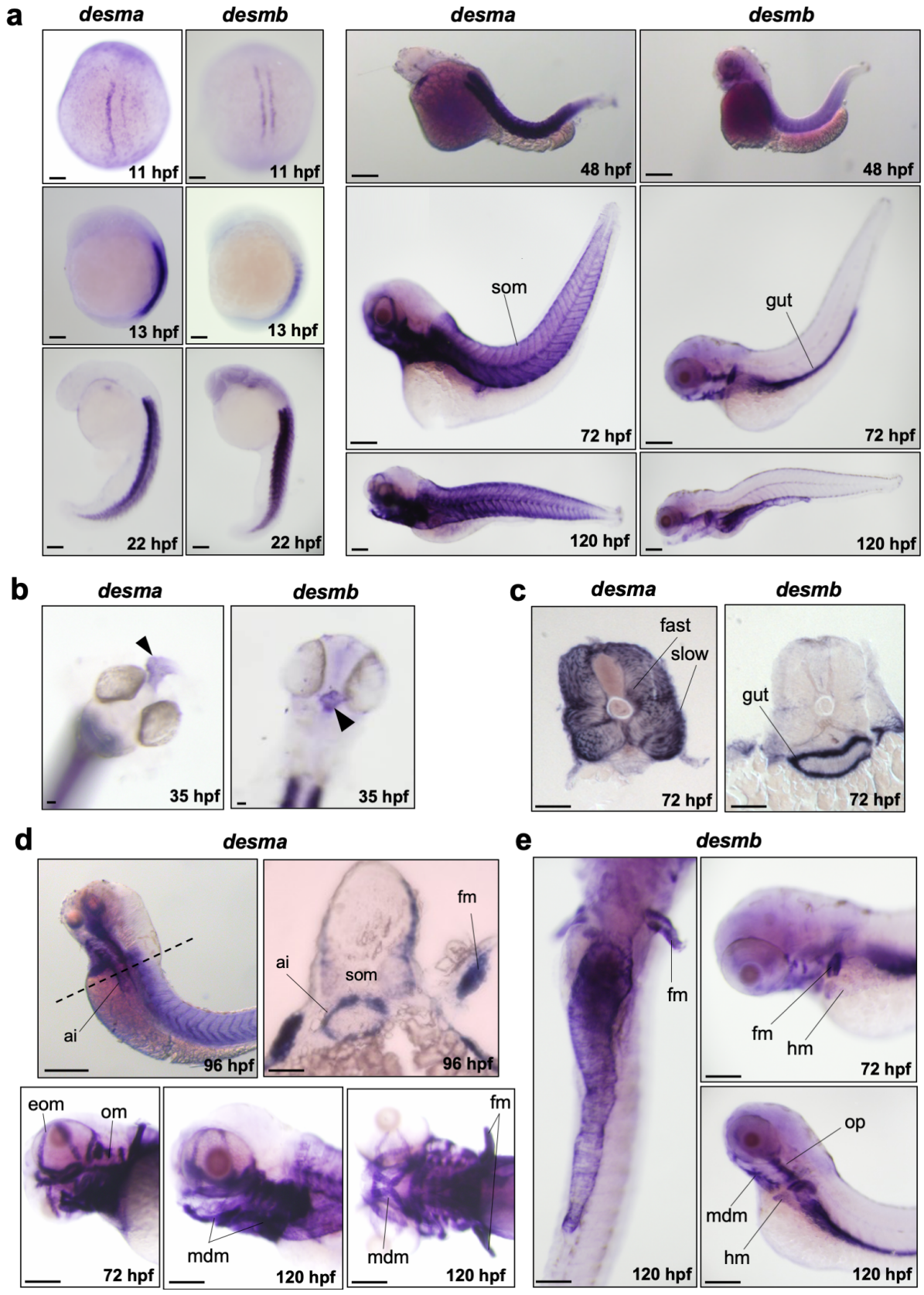

581

Figure 2.

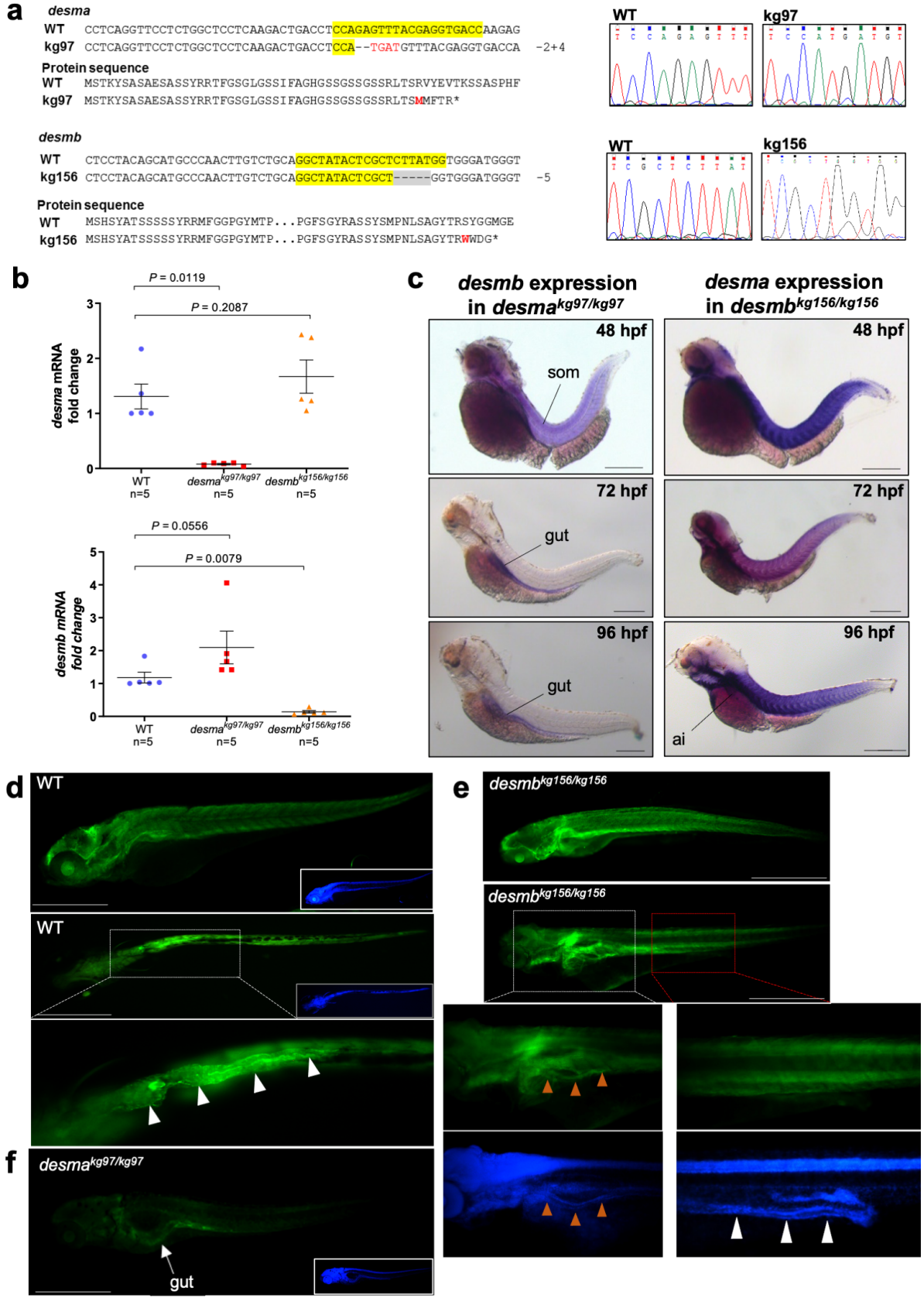

Figure 3.

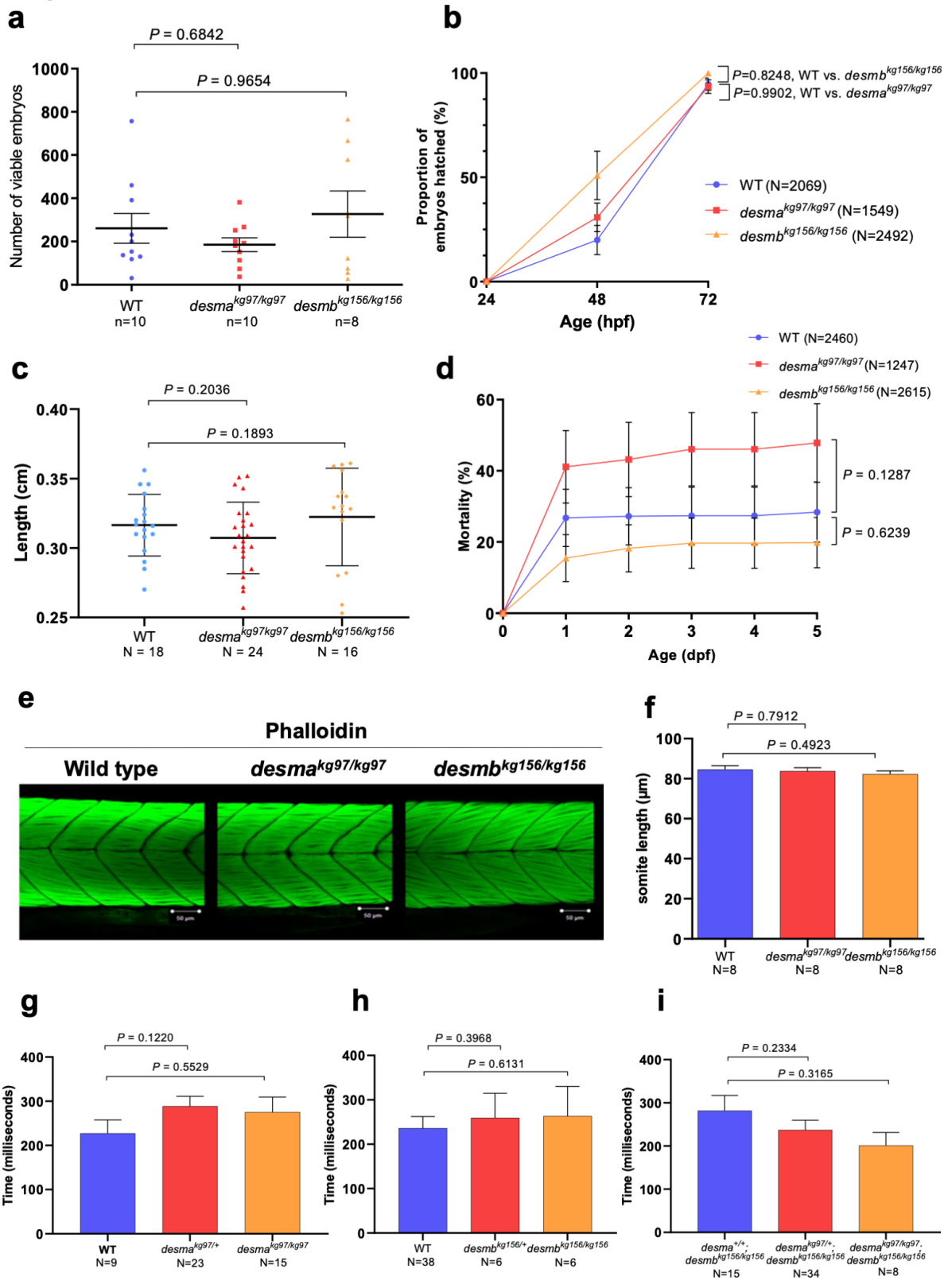

583

Figure 4.

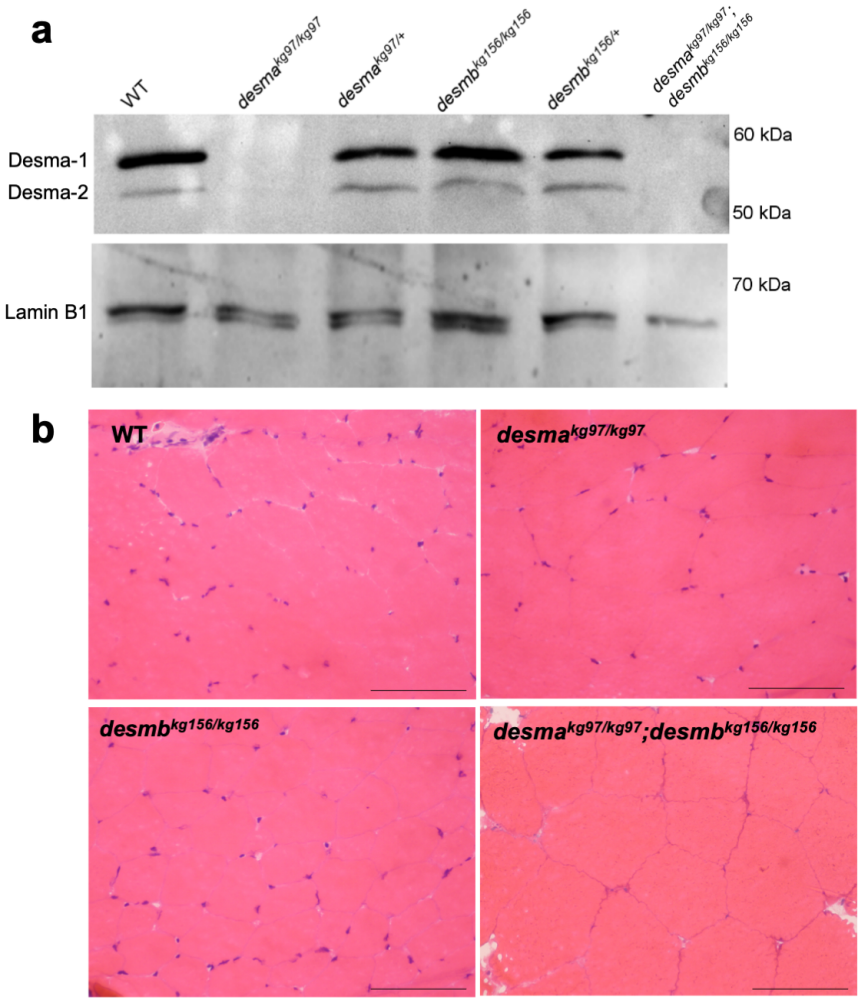

Figure 5.

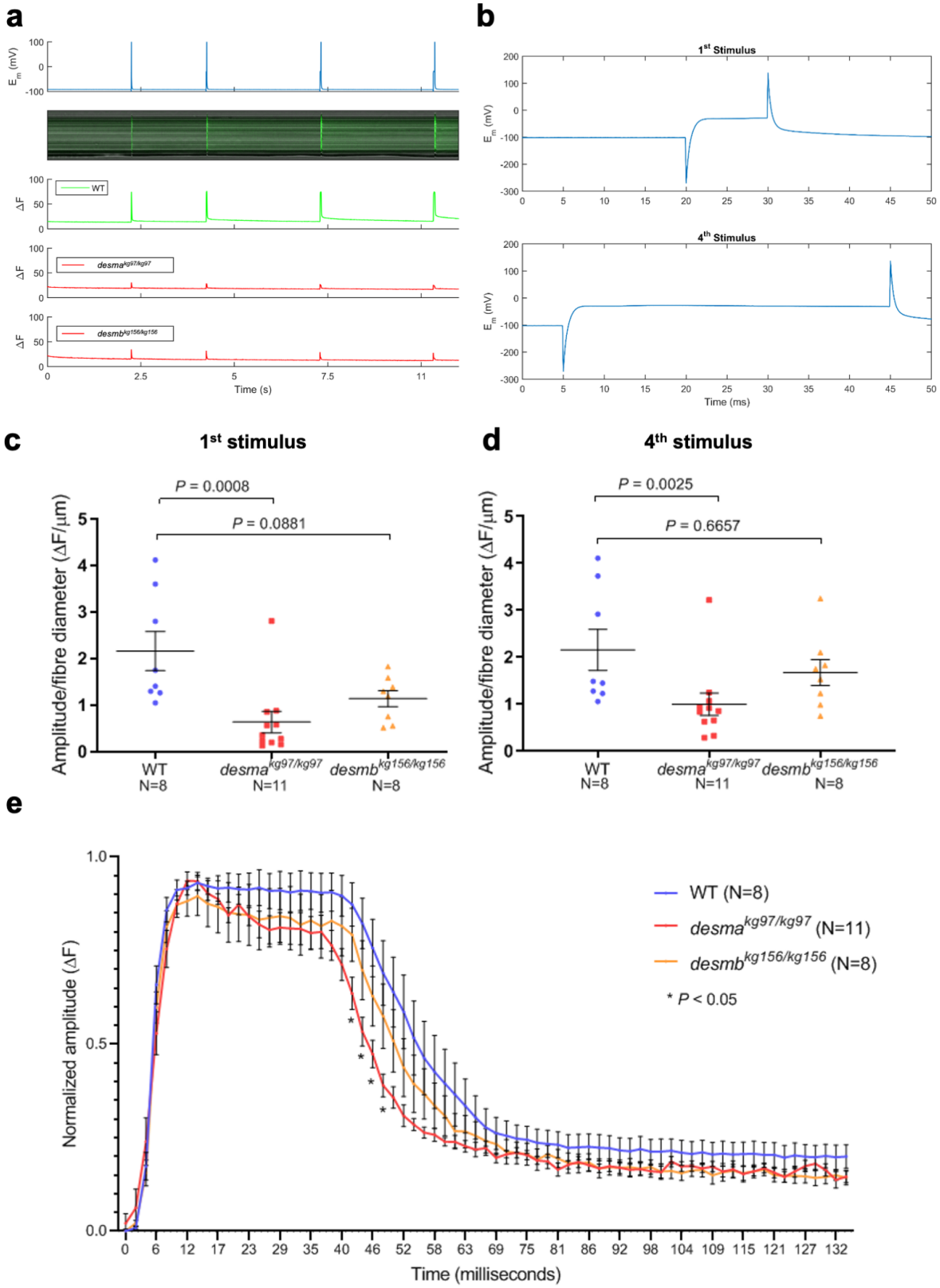

585